

# Optimization of growth conditions of type-II Zn(Cd)Te/ZnCdSe submonolayer quantum dot superlattices for intermediate band solar cells

Siddharth Dhomkar<sup>a)</sup> and Igor L. Kuskovsky<sup>b)</sup>

*Department of Physics, Queens College, CUNY, Flushing, New York 11367 and The Graduate Center, CUNY, New York, New York 10016*

Uttam Manna and I. C. Noyan

*Department of Applied Physics and Applied Mathematics, Columbia University, New York, New York 10027*

Maria C. Tamargo

*Department of Chemistry, City College of New York, CUNY, New York, New York 10031 and The Graduate Center, CUNY, New York, New York 10016*

(Received 21 November 2012; accepted 11 March 2013; published 21 March 2013)

Intermediate band solar cells (IBSCs) have been predicted to be significantly more efficient than the conventional solar cells, but have not been realized to their full potential due to the difficulties related to the fabrication of practical devices. The authors report here on growth and characterization of Zn(Cd)Te/ZnCdSe submonolayer quantum dot (QD) superlattices (SLs), grown by migration enhanced epitaxy. These QDs do not exhibit formation of wetting layers, which is one of the culprits for the unsatisfactory performance of IBSCs. The ZnCdSe host bandgap is  $\sim 2.1$  eV when lattice matched to InP, while the Zn(Cd)Te-ZnCdSe valence band offset is  $\sim 0.8$  eV. These parameters make this material system an excellent candidate for a practical IBSC. The detailed structural analysis demonstrates that the process of desorption of Cd and the preferential incorporation of Zn facilitates the formation of unintentional strained ZnSe-rich layer at the QD-spacer interface. The growth conditions have been then optimized so as to obtain high crystalline quality lattice matched SL, by growing intentionally Cd-rich spacers, which strain balanced the SL. The excitation intensity dependent photoluminescence confirmed the type-II nature of these multilayer QD structures, which is expected to suppress nonradiative Auger recombination, and improve the carrier extraction process when implemented in an actual device. © 2013 American Vacuum Society. [<http://dx.doi.org/10.1116/1.4797486>]

## I. INTRODUCTION

An intermediate band solar cell<sup>1</sup> (IBSC) is one of the most promising ways to increase the efficiency of a single-junction solar cell above the fundamental Shockley–Queisser limit.<sup>2</sup> IBSCs work on the principle of increasing the photocurrent by multiple transitions of either an electron or a hole, via introduction of an intermediate band (IB) of states within the forbidden band of the host semiconductor.<sup>3,4</sup> The efficiency of an optimal IBSC can be as high as 63% under full concentration, if the host bandgap is about 1.95 eV and the IB is at 0.71 eV (Refs. 1 and 4) from either the valence or the conduction band. The IB can be fabricated out of the confined levels in the semiconductor quantum dots (QDs); however, there are severe issues<sup>3,4</sup> associated with the availability of the material system with the parameters required for an optimal IBSC. Additionally, there are many challenges related to the growth mechanisms of the QD based IBSCs such as low QD density, formation of the wetting layer (WL), and the dislocations, arising due to accumulated strain.<sup>3,4</sup>

We have grown and characterized type-II Zn(Cd)Te/ZnCdSe submonolayer QDs, as a potential candidate for realization of a practical IBSC, and report the optimization of growth conditions. The Zn<sub>x</sub>Cd<sub>1-x</sub>Se host ( $x \sim 0.51$ ) lattice matched to InP has a bandgap of about 2.1 eV (Refs. 5 and 6) and Zn(Cd)Te

has a valence band offset of  $\sim 0.8$  eV (Refs. 7–11) with respect to ZnCdSe; therefore, an IB can be potentially fabricated at  $\sim 0.7$  eV from the hole ground states within Zn(Cd)Te QDs. The proximity of these parameters with those required for an ideal IBSC makes this material system a remarkable candidate for a successful practical device.

In order to examine and improve the growth mechanism of these QD superlattices (SLs), several samples were grown on the InP substrate by means of migration enhanced epitaxy (MEE), implementing various shutter sequences. The optical and structural characterization of these samples was then performed using photoluminescence (PL) and high resolution x-ray diffraction (HRXRD) analysis, respectively.

## II. EXPERIMENT

### A. Growth

The samples were grown epitaxially on (001) semi-insulating InP substrates in a RIBER 2300P molecular beam epitaxy system. Elemental In(7N), Ga(7N), and As(7N) were used for the InGaAs growth and elemental Zn(6N), Cd(7N), Se(6N), and Te(6N) were used for the growth of the QD multilayer structures. Oxide desorption of the InP substrates was performed in the III-V chamber by heating the substrates to a nominal substrate temperature of 530 °C with an As flux impinging on the surface to prevent P evaporation from the InP surface. Then, a 200 nm lattice matched InGaAs buffer layer was grown at a substrate temperature of

<sup>a)</sup>Electronic mail: [sdhomkar@qc.cuny.edu](mailto:sdhomkar@qc.cuny.edu)

<sup>b)</sup>Electronic mail: [Igor.Kuskovsky@qc.cuny.edu](mailto:Igor.Kuskovsky@qc.cuny.edu)

500 °C with a streaky ( $2 \times 4$ ) reflection high-energy electron diffraction (RHEED) pattern. The substrate with the InGaAs buffer layer was transferred to the II-VI chamber via transfer module under ultra high vacuum. Prior to the growth of the II-VI epilayers, the InGaAs surface was exposed to a Zn flux, followed by the growth of a ZnCdSe buffer layer at the substrate temperature of 180 °C. This step was intended to suppress the formation of Ga<sub>2</sub>Se<sub>3</sub> at the III-V/II-VI interface, which has been shown to result in the formation of stacking faults.<sup>12</sup> The ZnCdSe buffer layer was then grown at a nominal substrate temperature of 280 °C under Se rich conditions with a growth rate of  $\sim 0.4 \mu\text{m/h}$ . The RHEED pattern exhibited a streaky ( $2 \times 1$ ) reconstruction during the growth of buffer layer. A SL consisting of alternating QD and spacer layers was then grown on this buffer layer. Various QD SLs (samples A through D) were grown via MEE using various shutter sequences described in the following sections. It is important to note that in case of samples A, B, and D, only submonolayer quantities of Te were sequentially deposited between the ZnCdSe spacers during the MEE cycles. The growth interruptions facilitate enhanced surface migration and assist in the formation of self-assembled submonolayer Zn(Cd)Te QDs embedded in a ZnCdSe matrix.

### B. Characterization

Low temperature PL measurements were performed within a closed cycle refrigerating system. The 351 nm emission line of an Ar<sup>+</sup> laser was used as an excitation source, and the excitation intensity was varied by over four orders of magnitude using neutral density filters. The PL was dispersed through a third stage of a TriVista SP2 500i triple monochromator and was detected by a thermoelectrically cooled charge coupled device camera or a thermoelectrically cooled GaAs photomultiplier tube.

The HRXRD measurements were carried out at Beamline X20A at the National Synchrotron Light Source at the Brookhaven National Laboratory. All measurements were performed using monochromatic synchrotron radiation at 8 keV, with a double-crystal Ge (111) monochromator. To enhance the angular resolution, a Si (111) analyzer was placed in front of the detector.

## III. RESULTS AND DISCUSSION

### A. Growth of QDs without wetting layers

Sample A was grown with the shutter sequence shown in Fig. 1(a). A ZnCdSe spacer (nominally eight monolayers) was first grown, followed by a 5 s of growth interruption, during which all the shutters were closed to smoothen the surface and to desorb the excess Se. The ZnTe-rich QDs were then grown by a sequential deposition of the elements, involving three identical deposition cycles. In each cycle, the Zn shutter was first opened for 5 s, followed by 5 s with all the shutters closed, and then the Te shutter was opened for 5 s, again followed by 5 s with all the shutters closed. After repeating this cycle three consecutive times, the next ZnCdSe spacer layer was grown. The whole sequence of the growth of the ZnCdSe spacer and ZnTe QDs was then repeated 150 times to achieve a multilayered structure as illustrated in Fig. 1(b). The submonolayer ZnTe-rich QDs grow via a Volmer-Weber growth mode, without the formation of a ZnTe WL. The growth procedure and the grown QD multilayer structures have been extensively studied and reported previously for similar material systems.<sup>13–17</sup> The formation of WL, which is inherent to the Stranski–Krastanov growth mode QDs, tends to reduce the open circuit voltage in an IBSC and is hence regarded as one of the important drawbacks related to the fabrication, especially for prototype

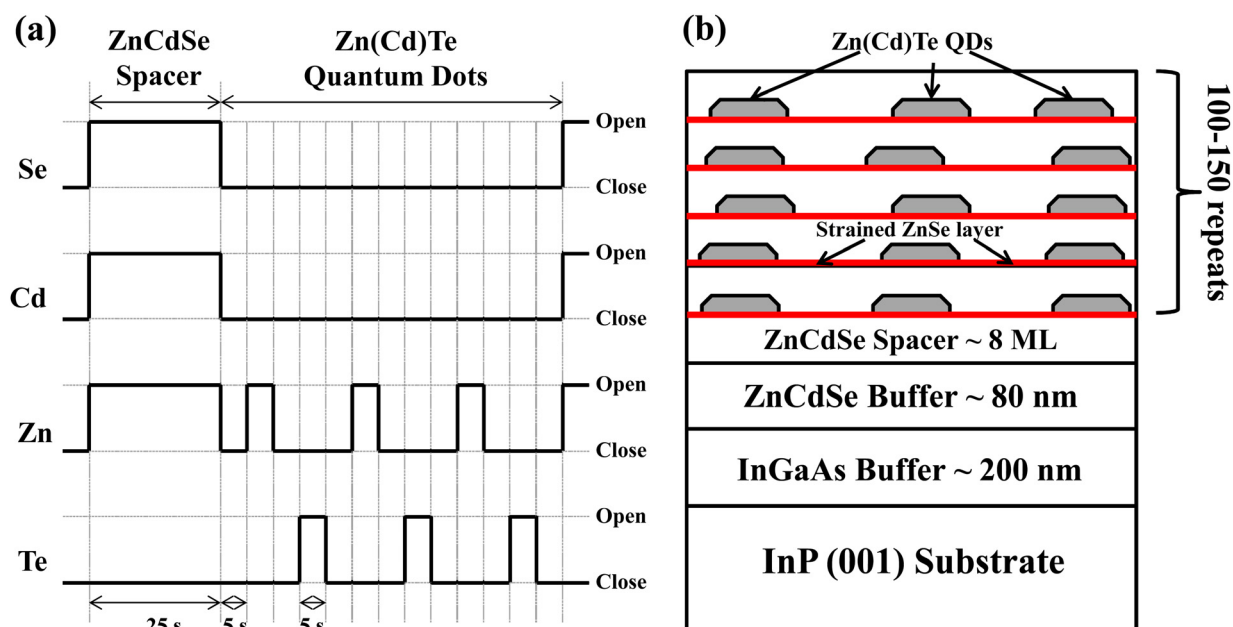


FIG. 1. (Color online) (a) MEE shutter sequence used during the growth of sample A. (b) Schematic diagram of a typical submonolayer Zn(Cd)Te/ZnCdSe QD SL.

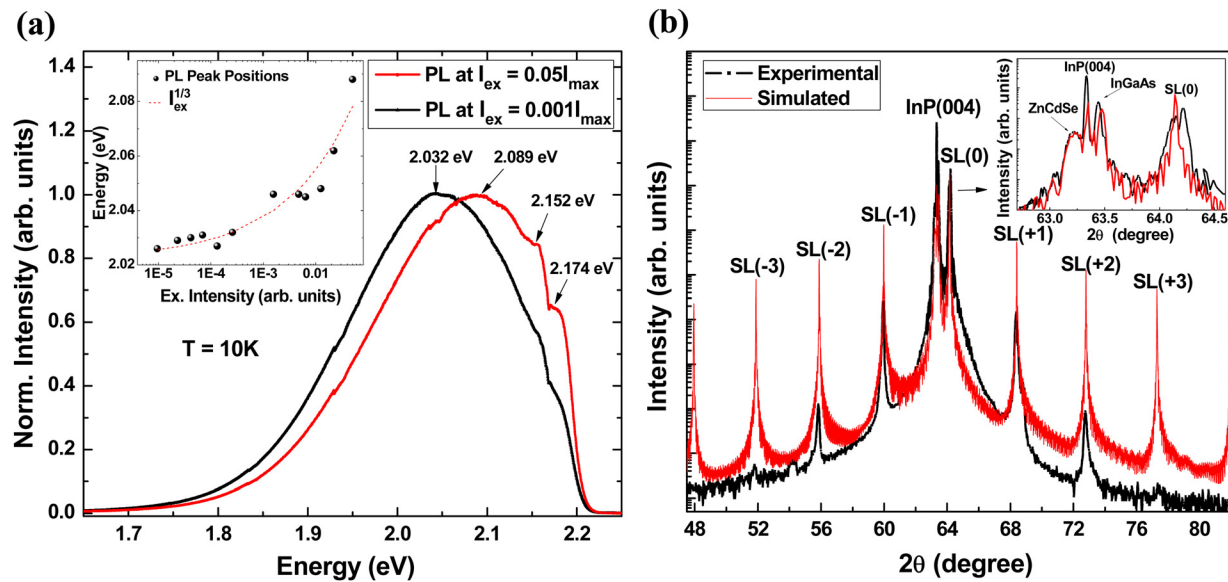


Fig. 2. (Color online) (a) PL spectra of sample A at 10 K for two different excitation intensities. Inset: The plot of PL peak positions at 10 K for various excitation intensities; the dashed line represents the fitted curve with cube root of excitation intensity. (b) Experimental and simulated HRXRD plots for sample A along the (004) reflection. Inset: HRXRD peaks corresponding to the substrate, two buffer layers and SL(0).

QD-IBSC system such as InAs/GaAs.<sup>3</sup> The formation of QDs without the WLS in these samples is expected to enhance the efficiency of an IBSC substantially.<sup>3</sup> Moreover, due to the submonolayer QDs, a SL can be grown with more than 100 periods avoiding strain induced dislocations. Thus, a stable multilayer structure can be fabricated with a large number of embedded QDs, which should increase the photocurrent notably.

## B. Type-II Zn(Cd)Te/ZnCdSe heterostructures

In order to study the type-II nature of this heterostructure, excitation intensity dependent PL studies were performed at low temperature [see Fig. 2(a)]. A strong red shift of the PL peak was observed with decreasing excitation intensity, which is a signature of type-II nanostructures.<sup>13,18–21</sup> The PL peak positions follow the fit of the cube root of the excitation intensity as shown in the inset of Fig. 2(a). This behavior is attributed to the band bending mechanism at the QD-spacer interface as a result of the spatial separation of photoexcited electrons and holes.<sup>13</sup> Due to the spatially indirect excitons in this heterostructure, nonradiative Auger<sup>22</sup> recombinations are expected to be suppressed and in turn enhance the process of carrier extraction significantly.<sup>23</sup>

## C. Structural analysis

### 1. Sample A

The results of the HRXRD for sample A are shown in Fig. 2(b). Sample A was found to be of high crystalline

quality as indicated by sharp and streaky RHEED pattern throughout the growth. In spite of obtaining high quality periodic SL satellite peaks in the HRXRD plot [see Fig. 2(b)], a relatively high, tensile lattice mismatch ( $\sim -1.2\%$ ) was observed between the 0th order SL peak (SL(0)) and the substrate peak. The high tensile mismatch seen in the HRXRD was unexpected as the ZnCdSe spacers were almost lattice matched to the InP substrate, and any mismatch introduced by the presence of the QDs is expected to be compressive, since ZnTe is compressively mismatched to InP with a mismatch of  $\sim 3.7\%$ . In order to investigate the structural properties and mechanisms leading to this mismatch, the HRXRD curve along the (004) reflection was simulated by a commercially available BEDE RADS program based on Takagi<sup>24</sup> and Taupin<sup>25</sup> generalized dynamical theory. To simulate the plots, the QDs were substituted by an effective layer with the same structure factor as that of the QD material, after taking into account some Se diffusion. The initialization of the simulation parameters was done based on the HRXRD simulations performed on similar material systems.<sup>18,26</sup> The results are shown in Table I.

The simulation suggests the presence of an unintentional pseudomorphic ZnSe-rich interfacial layer (IL), about a monolayer thick, forming at the QD-spacer interface. This IL was thought to be originating from any one of the several possible steps: (i) the Se terminated surface after the growth of the ZnCdSe spacer, which might be forming ZnSe upon Zn exposure during MEE, (ii) the background Se pressure, as the sample was grown in Se-rich conditions, and (iii) the

TABLE I. Summary of the material parameters for sample A obtained from the simulation.

Sample	SL period (nm)	Spacer composition	IL composition	IL thickness (nm)	QD composition
A	2.38	Zn <sub>0.49</sub> Cd <sub>0.51</sub> Se <sub>0.99</sub> Te <sub>0.01</sub>	ZnSe <sub>0.97</sub> Te <sub>0.03</sub>	0.31	ZnTe <sub>0.5</sub> Se <sub>0.5</sub>

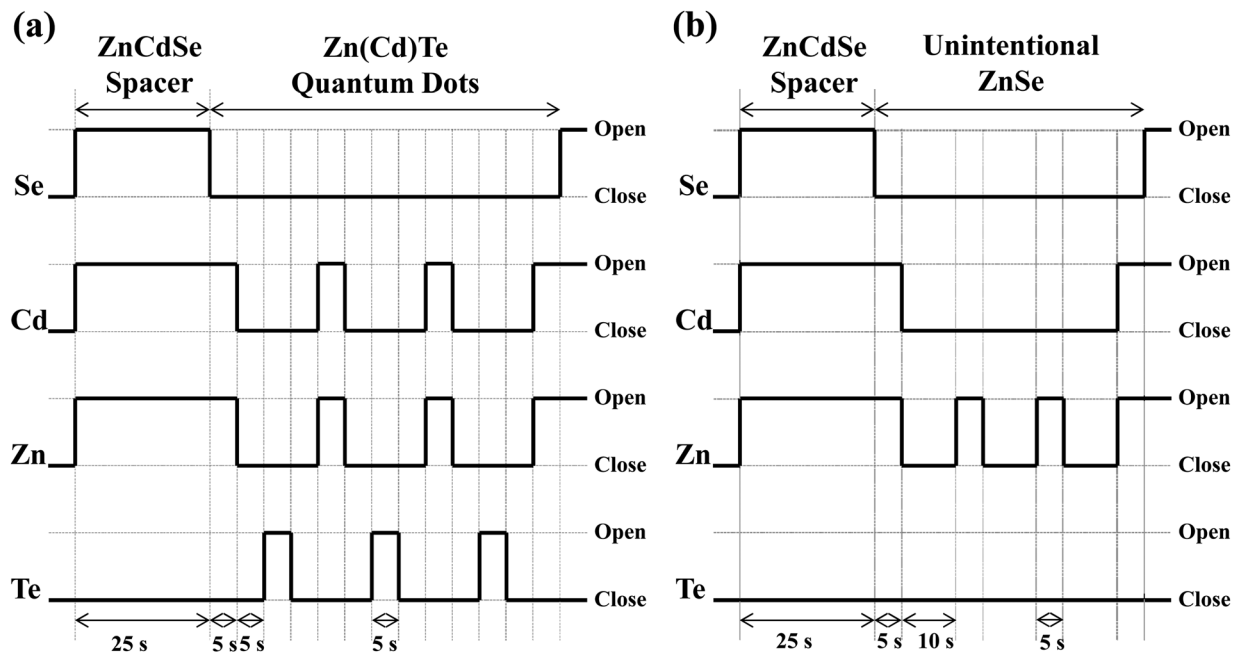


FIG. 3. MEE shutter sequence used during the growth of (a) sample B and (b) sample C.

desorption of Cd from the ZnCdSe spacer during MEE, due to low or no Se flux. While this IL did not adversely affect the optical properties of the structure, the large lattice mismatch of the SL may introduce undesirable degradation effects during future device operation.

## 2. Samples B and C

In order to understand the mechanism leading to the formation of the ZnSe-rich IL, samples B and C were grown by the modified shutter sequences illustrated in Fig. 3. During the growth of sample B, the Zn and Cd shutters were kept open for 5 s after the growth of the ZnCdSe spacer to terminate the surface with group II elements instead of Se. This was intended to avoid the formation of ZnSe after Zn exposure in the first cycle of MEE. Also, the Cd shutter was opened along with the Zn shutter during MEE so that if there is any Se present at any time, a ZnCdSe layer would form rather than a ZnSe layer. A clear change in the RHEED pattern from  $(2 \times 1)$  to  $C(2 \times 2)$  was indeed observed prior to the formation of QDs and during MEE, indicating the complete surface coverage by group II elements (see Fig. 4). Although the surface was terminated with the group II elements, the presence of ZnSe-rich strained layer at the QD-spacer interface was again confirmed by HRXRD as shown in Fig. 5(a). The mismatch between SL(0) and the substrate peak was found to be almost the same as that of the sample A. This result eliminated the possibilities related to the surface termination by Se and to the excess Se pressure, while it pointed toward Cd desorption being the main reason behind the formation of the IL.

Sample C was then grown without opening Te shutter during MEE, hence shortening MEE cycles, to confirm that the process of the formation of the strained ZnSe IL is independent of that of the ZnTe QDs formation, and to corroborate the

role of Cd desorption in the growth. For sample C, the lattice mismatched SL peak along with the periodic satellite peaks was observed in HRXRD plot [see Fig. 5(b)], indicating the presence of unintentional ZnSe/ZnCdSe SL. The fact that the lattice mismatch between SL(0) and the substrate peak is lower than that of sample A and B suggests that the mismatch is proportional to the duration of the MEE cycles. This result also supports the likelihood of Cd desorption as the cause for formation of the ZnSe-rich IL.

Additionally, it is known<sup>27</sup> that the incorporation rate of Cd is lower than that of Zn, and approaches zero at very low Se fluxes. As a result of the difference in the incorporation

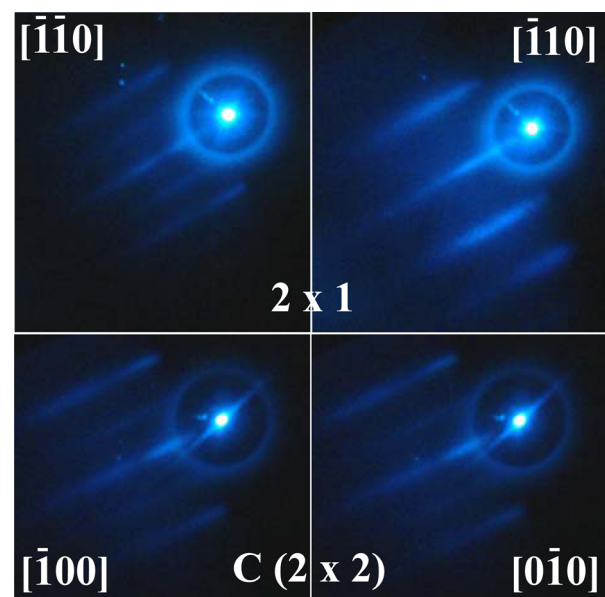


FIG. 4. (Color online) RHEED reconstruction pattern during the growth of ZnCdSe spacer (top) and Zn(Cd)Te QDs (bottom).

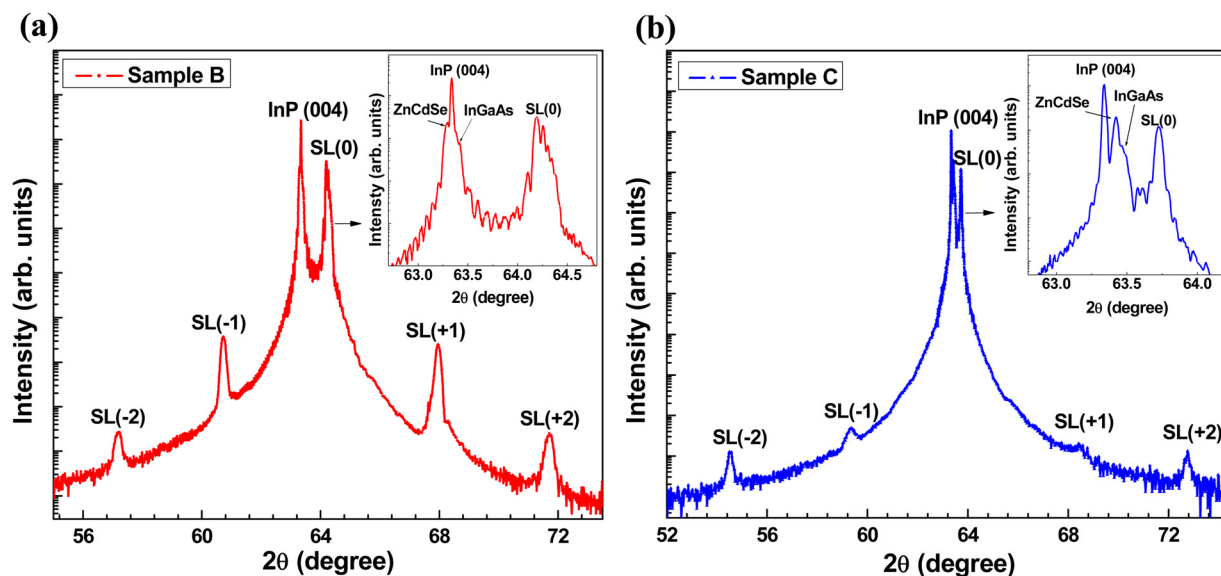


Fig. 5. (Color online) Experimental HRXRD plots along (004) reflection for (a) sample B, and (b) sample C. Inset: HRXRD peaks corresponding to the substrate, two buffer layers and SL(0).

rates of these elements, Zn replaces Cd during the growth and gets preferentially incorporated when grown under low or no Se conditions. Moreover, the previous report<sup>27</sup> supports the observation of increased Cd desorption rates at low Se fluxes. This led us to deduce that the Cd desorption together with the preferential incorporation of Zn is leading to the formation of an unintentional strained ZnSe-rich IL at the QD-spacer interface.

### 3. Sample D

Based on the observations from samples B and C, we concluded that the formation of ZnSe-rich IL cannot be easily

avoided during the MEE process. Hence, in order to grow a high quality lattice matched SL with more periods, the approach of strain balancing was chosen. To achieve this, sample D was then grown with the same shutter sequence as that of the sample B, but with the smaller wait time (3 s) between opening of Zn, Cd, and Te shutters to minimize the desorption of Cd during MEE. Most importantly, intentionally Cd-rich spacer layers were grown in order to compensate the strain introduced by the unintentional ZnSe-rich IL. By carefully adjusting the Cd content in  $Zn_xCd_{1-x}Se$ , we were able to obtain a high quality nearly lattice matched SL, as confirmed by the HRXRD [see Fig. 6(a)]. The intentionally lattice mismatched pseudomorphic  $Zn_xCd_{1-x}Se$  buffer with

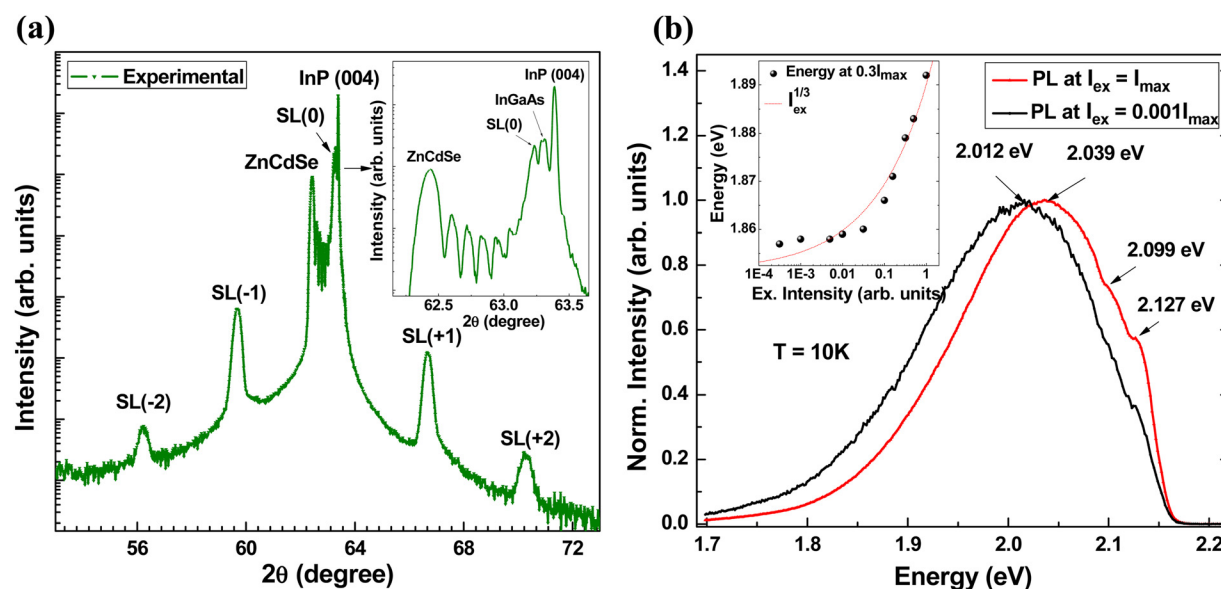


Fig. 6. (Color online) (a) Experimental HRXRD plot for sample D along (004) reflection. Inset: HRXRD peaks corresponding to the substrate, two buffer layers and SL(0). (b) The PL spectra of sample D at 10 K for two different excitation intensities. Inset: The plot of PL energy at 30% of the PL peak at 10 K for various excitation intensities; the dashed line represents the fitted curve with cube root of excitation intensity.

the same composition as that of the spacer was grown prior to the growth of the SL in order to measure the spacer composition required for the lattice matched SL and its bandgap. In spite of being lattice mismatched, the buffer layer was observed to be of high crystalline quality as indicated by the observation of RHEED oscillations during the growth and the thickness fringes in the HRXRD plot, shown in Fig. 6(a). The lattice mismatch in the growth direction of the buffer layer with InP was found to be  $\sim 1.35\%$ , and the thickness was calculated to be about 90 nm from the thickness fringes and the RHEED oscillations. Using this information and assuming a linear dependence of the lattice parameter (Vegard's law), the buffer layer composition was estimated to be  $\text{Zn}_{0.41}\text{Cd}_{0.59}\text{Se}$ . Furthermore, the room temperature bandgap corresponding to this buffer layer composition was evaluated to be 2.01 eV, using the known band bowing parameter.<sup>5</sup> This host bandgap is expected to increase by about 18 meV due to compressive strain in the system, calculated using deformation potentials<sup>28</sup> for this particular ternary alloy composition. Thus, introduction of a Cd-rich spacer in the SL lowered the spacer bandgap and brought it even closer to that of the ideal IBSC host, besides assisting in the growth of lattice matched SL. This result also illustrates an added advantage of this material system, which is the ability to carefully engineer the IBSC materials by strain balancing to achieve the ideal band structure and the material properties.

The excitation intensity dependent PL at 10 K showed a shift in PL energy [see Fig. 6(b)] similar to sample A, demonstrating the type-II nature of the multilayered structure. The PL also showed phonon replicas, separated by the  $\text{Zn}_{0.41}\text{Cd}_{0.59}\text{Se}$  longitudinal-optical-phonon energy,<sup>28</sup> indicating small amounts of Te diffusion into the spacers and high crystalline quality of the QD SL. Hence, we were able to retain desirable optical properties of this material system, while improving the crystalline quality of the SL by strain balancing technique. Finally, a typical band line-up for this material system has been drawn (see Fig. 7) considering same spacer composition as that of the sample D and with a 1 nm thick  $\text{ZnCd}_{0.2}\text{Te}_{0.8}$  QD. The band diagram has been simplified by ignoring ZnSe IL, as this layer does not influence the optical properties due to negligible change in the valence band offset. For the calculation purpose,

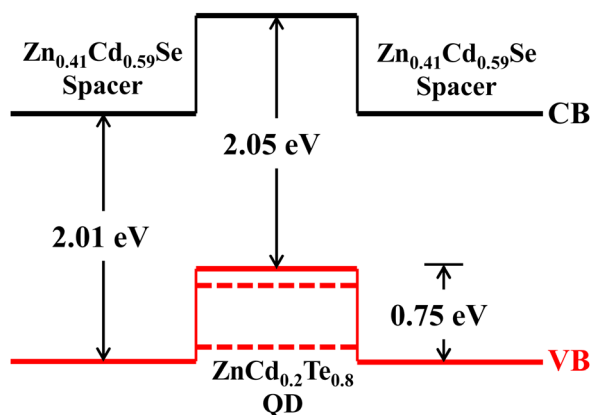


Fig. 7. (Color online) Typical band line-up for a 1 nm thick  $\text{ZnCd}_{0.2}\text{Te}_{0.8}$  QD embedded in the  $\text{Zn}_{0.41}\text{Cd}_{0.59}\text{Se}$  spacer.

one-dimensional Schrodinger equation was solved using the reported values of valence band offsets<sup>7–11</sup> and hole effective masses.<sup>7,29</sup>

#### IV. SUMMARY AND CONCLUSIONS

Type-II Zn(Cd)Te/ZnCdSe submonolayer QD SLs were grown epitaxially without the formation of wetting layer and were characterized via PL and HRXRD. The systematic HRXRD analysis of several samples grown with different shutter sequences during the MEE allowed us to conclude that the process of desorption of Cd along with the favored incorporation of Zn due to absence of Se flux during MEE was resulting in the formation of a strained ZnSe-rich IL at the QD-spacer interface. Another sample (sample D) was then grown with an intentional Cd-rich  $\text{Zn}_{0.41}\text{Cd}_{0.59}\text{Se}$  spacer in order to balance the strain produced by this ZnSe-rich IL, and consequently, a high quality SL, lattice matched to the substrate, was obtained. The type-II nature of the optimized sample was established from the clear red shift in the PL spectra with decrease in excitation intensity at 10 K and a typical band alignment for this material system has been presented. Owing to its appropriate optical properties and bandgaps, as well as the optimized growth mechanism and the possibility of strain balancing, this material system is a very promising candidate to fabricate an ideal IBSC.

#### ACKNOWLEDGMENTS

This research was supported by the U. S. Department of Energy, Office of Basic Energy Sciences, Division of Materials Sciences and Engineering under Award No. DE-FG02-10ER46678. Use of the National Synchrotron Light Source, Brookhaven National Laboratory, was supported by the U.S. Department of Energy, Office of Science, Office of Basic Energy Sciences, under Contract No. DE-AC02-98CH10886.

<sup>1</sup>A. Luque and A. Martí, *Phys. Rev. Lett.* **78**, 5014 (1997).

<sup>2</sup>W. Shockley and H. J. Queisser, *J. Appl. Phys.* **32**, 510 (1961).

<sup>3</sup>A. Luque and A. Martí, *Adv. Mater.* **22**, 160 (2010).

<sup>4</sup>A. Luque, A. Martí, and C. Stanley, *Nature Photon.* **6**, 146 (2012).

<sup>5</sup>Y. D. Kim, M. V. Klein, S. F. Ren, Y. C. Chang, H. Luo, N. Samarth, and J. K. Furdyna, *Phys. Rev. B* **49**, 7262 (1994).

<sup>6</sup>U. Lutz, J. Kuhn, F. Goschenhofer, U. Schüssler, S. Einfeldt, C. R. Becker, and G. Landwehr, *J. Appl. Phys.* **80**, 6861 (1996).

<sup>7</sup>W. Faschinger, S. Ferreira, and H. Sitter, *Appl. Phys. Lett.* **64**, 2682 (1994).

<sup>8</sup>J. Puls, M. Rabe, H.-J. Wünsche, and F. Henneberger, *Phys. Rev. B* **60**, R16303 (1999).

<sup>9</sup>H. J. Lozykowski and V. K. Shastri, *J. Appl. Phys.* **69**, 3235 (1991).

<sup>10</sup>D. J. Milliron, S. M. Hughes, Y. Cui, and L. Manna, *Nature* **430**, 190 (2004).

<sup>11</sup>S. Kim, B. Fisher, H.-J. Eisler, and M. Bawendi, *J. Am. Chem. Soc.* **125**, 11466 (2003).

<sup>12</sup>D. Li and M. D. Pashley, *J. Vac. Sci. Technol. B* **12**, 2547 (1994).

<sup>13</sup>Y. Gu, I. L. Kuskovsky, M. van der Voort, G. F. Neumark, X. Zhou, and M. C. Tamargo, *Phys. Rev. B* **71**, 045340 (2005).

<sup>14</sup>I. L. Kuskovsky, W. MacDonald, A. O. Govorov, L. Mourokh, X. Wei, M. C. Tamargo, M. Tadic, and F. M. Peeters, *Phys. Rev. B* **76**, 035342 (2007).

<sup>15</sup>B. Roy, A. Shen, M. C. Tamargo, and I. L. Kuskovsky, *J. Electron. Mater.* **40**, 1775 (2011).

- <sup>16</sup>B. Roy, H. Ji, S. Dhomkar, F. J. Cadieu, L. Peng, R. Moug, M. C. Tamargo, and I. L. Kuskovsky, *Appl. Phys. Lett.* **100**, 213114 (2012).
- <sup>17</sup>U. Manna, Q. Zhang, S. Dhomkar, I. F. Salakhutdinov, M. C. Tamargo, I. C. Noyan, G. F. Neumark, and I. L. Kuskovsky, *J. Appl. Phys.* **112**, 063521 (2012).
- <sup>18</sup>Y. Gong, H. F. Yan, I. L. Kuskovsky, Y. Gu, I. C. Noyan, G. F. Neumark, and M. C. Tamargo, *J. Appl. Phys.* **99**, 064913 (2006).
- <sup>19</sup>E. R. Glaser, B. R. Bennett, B. V. Shanabrook, and R. Magno, *Appl. Phys. Lett.* **68**, 3614 (1996).
- <sup>20</sup>F. Hatami *et al.*, *Phys. Rev. B* **57**, 4635 (1998).
- <sup>21</sup>N. N. Ledentsov *et al.*, *Phys. Rev. B* **52**, 14058 (1995).
- <sup>22</sup>G. G. Zegrya and A. D. Andreev, *Appl. Phys. Lett.* **67**, 2681 (1995).
- <sup>23</sup>H. Zhu, N. Song, W. Rodríguez-Córdoba, and T. Lian, *J. Am. Chem. Soc.* **134**, 4250 (2012).
- <sup>24</sup>S. Takagi, *Acta Crystallogr.* **15**, 1311 (1962).
- <sup>25</sup>D. Taupin, *Bull. Soc. Fr. Mineral. Cristallogr.* **87**, 469 (1964).
- <sup>26</sup>U. Manna *et al.*, *J. Appl. Phys.* **111**, 033516 (2012).
- <sup>27</sup>H. Okuyama, S. Kijima, Y. Sanaka, and A. Ishibashi, *J. Cryst. Growth* **193**, 43 (1998).
- <sup>28</sup>Z. Z. Guo, X. X. Liang, and S. L. Ban, *Phys. Status Solidi B* **238**, 173 (2003).
- <sup>29</sup>E. Tyrrell and J. Smith, *Phys. Rev. B* **84**, 165328 (2011).